Preparation, magnetism and electronic structures of cadmium technetates†‡

Efrain E. Rodriguez,*[ab] Frédéric Poineau,[c] Anna Llobet,[b] Joe D. Thompson,[d] Ram Seshadri[e] and Anthony K. Cheetham[f]

Received 30th July 2010, Accepted 3rd October 2010
DOI: 10.1039/c0jm02470h

Due to the scarcity of the artificial transition metal technetium, studies on the solid-state properties of its oxides have been rarely undertaken. We have prepared a new technetium metal oxide system that include the *4d* metal in two separate oxidation states and have characterized the new phases' crystal structures and magnetic properties. One phase $Cd_2Tc_2O_7$ was prepared through the vapor-phase reaction of the heptaoxide Tc_2O_7 with Cd metal; the other phase, $CdTcO_3$, was prepared through the solid state reaction of TcO_2 with CdO. High-resolution synchrotron X-ray diffraction was used to characterize the crystal structures and stoichiometries of the two new technetates. At room temperature, $Cd_2Tc_2O_7$ takes on the pyrochlore structure with $a = 10.18118(1)$ Å, space group, $Fd\bar{3}m$ and $Z = 8$. $CdTcO_3$ has the $GdFeO_3$-type structure with space group *Pbnm* and $a = 5.38881(1)$ Å, $b = 5.46504(1)$ Å, and $c = 7.71272(1)$Å. The magnetic susceptibility behavior of $Cd_2Tc_2O_7$ is strikingly similar to that observed in $Cd_2Re_2O_7$, with a broad transition close to 200 K. The magnetic behavior of $Cd_2Tc_2O_7$ is also compared with that of isomorphous $Pb_2Tc_2O_6$ and $Bi_2Tc_2O_7$, also presented in this study. The magnetic susceptibility of the distorted perovskite phase $CdTcO_3$ is weakly temperature dependent, with no obvious signs of an ordering transition below 300 K. Electronic band structure calculations performed to simulate electronic densities of states indicate that the Fermi level is located in a 't_{2g}' band of the octahedrally coordinated Tc cations and therefore metallic conductivity in both $CdTcO_3$ and $Cd_2Tc_2O_7$.

1 Introduction

Among the various subsets of inorganic materials, transition metal oxides have captured the imagination and interest of materials scientists, chemists, and physicists for their diverse physical and chemical properties. Among investigations of electronic properties of transition metal oxides, those on oxides containing ruthenium have produced a wide array of physical phenomenon. The Ru-containing oxides, or ruthenates, can express properties such as superconductivity in Sr_2RuO_4, collective electron ferromagnetism in $SrRuO_3$, and metal-to-insulator (MI) transitions in several $A_2Ru_2O_7$ compounds (where A is a divalent cation).[1] Typically, in the latter compounds, Ru is paired with a heavy post-transition metal as in $Tl_2Ru_2O_7$ or $Hg_2Ru_2O_7$. In the case of $Tl_2Ru_2O_7$, an interesting one-dimensional ordering of the Ru d orbitals within the three-dimensional crystal structure leads to the MI transition,[2,3] while in $Hg_2Ru_2O_7$, the MI transition is thought to be purely electronic.[4,5] These fascinating electronic and structural properties in the Sr–Ru–O system and the ruthenate pyrochlores motivated our study of mixed-metal oxides of neighboring 4*d* metal, technetium, an artificial element often overlooked due to its paucity.

For the first time in over 40 years, mixed-metal oxides containing Tc were prepared in a study on the oxides $Bi_2Tc_2O_7$, Bi_3TcO_8, and $Bi_3Tc_3O_{11}$.[6] In the present study, two new Tc-containing oxides with another post-transition metal, cadmium, are presented. Unlike Bi^{3+} and Pb^{2+}, Cd^{2+} is a smaller and less polarizable cation due to its higher charge density. Furthermore, the stereochemical effect of an inert pair of s electrons does not play a role in the crystal chemistry of Cd^{2+} as it does for Bi^{3+} and Pb^{2+}. While not as electropositive as the alkaline earth metals, Cd is more so than Bi and Pb, which should also influence the bonding interaction between the Tc and O atoms.

The pyrochlore structure has been found to occur for oxides with the stoichiometry $Cd^{2+}{}_2M^{5+}{}_2O_7$ where M = Nb, Ta, Ru, Re, Os, and Ir.[7] These Cd-containing oxides of the 4*d*/5*d* series have shown a diverse array of electronic behavior. $Cd_2Nb_2O_7$ and $Cd_2Ta_2O_7$ are insulating, as expected from the d^0 configuration, and in the case of the niobate, a complex ferroelectric transition occurs around 180 K.[8] Contrastingly, $Cd_2Re_2O_7$ was the first oxide with the pyrochlore structure found to exhibit superconductivity with a T_c around 1 K.[9–11] In the homologous oxide of neighboring osmium, a metal-to-insulator (MI) transition occurs instead around 225 K.[12,13] Since Tc and Re have similar chemistries, studying the structure and properties of the Tc analogue

[a]*NIST Center for Neutron Research, National Institute of Standards and Technology, Gaithersburg, MD, USA. E-mail: efrainr@nist.gov*
[b]*Manuel Lujan Neutron Scattering Center, Los Alamos National Laboratory, Los Alamos, New Mexico, 87545, USA*
[c]*Harry Reid Center for Environmental Studies, University of Nevada, Las Vegas, Nevada, 89154-4009, USA*
[d]*Materials Physics and Applications Division, Los Alamos National Laboratory, Los Alamos, New Mexico, 87545, USA*
[e]*Materials Department and Materials Research Laboratory, University of California, Santa Barbara, CA, 93106, USA*
[f]*Department of Materials Science and Metallurgy, University of Cambridge, Pembroke Street, Cambridge, CB2 3QZ, UK*
† Electronic supplementary information (ESI) available: Further details. See DOI: 10.1039/c0jm02470h
‡ This paper is part of a *Journal of Materials Chemistry* themed issue in celebration of the 70th birthday of Professor Fred Wudl.

would be imperative for further exploring the phenomena of superconductivity and MI transitions in 4*d*/5*d* oxides with the pyrochlore structure. Consequently, we have, for the first time, prepared the oxides $Cd_2Tc_2O_7$ and $CdTcO_3$, with the former adopting the pyrochlore structure and the latter a distorted perovskite structure.

In $Cd_2Tc_2O_7$, the Tc^{5+} cations have a $4d^2$ configuration, whereas in $CdTcO_3$, the Tc^{4+} cations have a $4d^3$ configuration, an interesting state to explore since it might correspond to a half-filled t_{2g} manifold in an octahedral crystal field, and thus a possible instability leading to magnetic ordering. The preparation of the two new cadmium technetates is presented along with high-resolution synchrotron X-ray diffraction (XRD) data to characterize their crystal structures. The magnetic properties of $CdTcO_3$ and $Cd_2Tc_2O_7$ as characterized from SQUID magnetometry measurements are also presented. Finally, electronic structure calculations for the two Cd–Tc–O phases were performed in order to predict possible electronic transport behavior.

2 Experimental

[Caution: ^{99}Tc is radioactive with a specific activity of 17 mCi/gram. To prevent contamination and ensure personal safety, standard practices of a radiochemistry laboratory must be followed.]

The $CdTcO_3$ phase was prepared by heating a stoichiometric mixture of CdO and TcO_2 at 850 °C in a fused quartz boat under flowing Ar gas for 12 h. TcO_2 was prepared by thermal decomposition of NH_4TcO_4 as described in previous work.[14] The resulting powder, which appears light grey metallic, was treated with 2M HCl to remove any remaining CdO and subsequently washed with water and acetone. Preliminary powder XRD data showed a pattern with Bragg peaks matching the orthorhombic lattice of the perovskite $CdTiO_3$.

For the preparation of $Cd_2Re_2O_7$, Donohue *et al.*[15] reacted ReO_3 with CdO in a sealed quartz ampoule at 1000 °C. They suggested the preparation of the pyrochlore oxide occurred through a redox reaction where CdO was reduced to Cd metal and ReO_3 oxidized to Re_2O_7; the products then volatilized to the cooler end of the tube and combined to produce purple metallic crystals of $Cd_2Re_2O_7$. Indeed, He *et al.*[16] grew single crystals through slow vapor phase reaction of Re_2O_7 and Cd metal. Similarly, we used Tc_2O_7 as a starting material to react with Cd metal cleaned with 2M HCl to remove any oxide on the surface. For the preparation of Tc_2O_7, TcO_2 was combusted in pure, dry oxygen in a sealed quartz ampoule heated to 450 °C for two hours. After complete oxidation of TcO_2 to Tc_2O_7, the tube was opened and a stoichiometric amount of Cd metal inserted (2 : 1 ratio for metal:Tc_2O_7). The reactants were heated to 800 °C under vacuum for ten hours and then furnace cooled. The product appeared as clusters of blue-green metallic crystals. Lacking a quality single crystal, the product was cleaned with 2M HCl and ground into a powder. The XRD powder pattern indicated a highly crystalline, cubic cell with Bragg peaks matching those of $Cd_2Re_2O_7$.

The powder patterns of $CdTcO_3$ and $Cd_2Tc_2O_7$ were collected with the high-resolution beamline 11-BM diffractometer at the Advanced Photon Source at Argonne National Laboratory. Details concerning the high-resolution X-ray diffraction, SQUID magnetometry, and electronic band structure calculations can be found in Supplementary Information. Further details on sample preparation can also be found in the Supplementary Information.†

3 Results and discussion

3.1 Structural details

Using the GSAS software package,[17] the crystal structures of $Cd_2Tc_2O_7$ and $CdTcO_3$ were refined with the room temperature, high-resolution powder XRD data. Starting with the structural parameters of $Cd_2Re_2O_7$, the Rietveld refinement with the 15 keV XRD data of $Cd_2Tc_2O_7$ converged to the parameters shown in Table 1 with an R_{wp} of 12.3% and χ^2 of 2.043. The R_{wp} is high due to the high-resolution and low background quality of the data, and is not necessarily an indication of an insufficient structural model. In Rietveld analysis, the χ^2 is similar to the goodness of fit G of the single crystal literature and equal to $(R_{wp}/R_{exp})^2$ where R_{exp} is the 'best' possible expected R_{wp} for a given data set.[18,19] Since χ^2 from our refinement is 2.043, then R_{wp} is only equal to about $1.42R_{exp}$, validating our model for the observed high-resolution, low background data. Furthermore, the accuracy of the model is apparent from the relatively smooth difference curve between the observed and calculated powder patterns for $Cd_2Tc_2O_7$ as shown in Fig. 1.

At room temperature, $Cd_2Tc_2O_7$ takes on the idealized pyrochlore structure (see Fig. 2) with $a = 10.18118(1)$ Å, space group $Fd\bar{3}m$ (origin choice 2), and $Z = 8$ formula units per cell. The high-resolution powder pattern also revealed some impurities in the powder with TcO_2 accounting for around 2.7 wt.% and $CdTcO_3$ around 1.5 wt.%. Unlike $Bi_2Tc_2O_{7-\delta}$, $Cd_2Tc_2O_7$ was found to be stoichiometric and with a much shorter Tc–O bond length of 1.926(1) Å than that found in TcO_2 (1.982 Å on average)[14] or in the other pyrochlore $Bi_2Tc_2O_{7-\delta}$ (2.0108 Å on average).[6] Thus the structural results confirm the presence of Tc^{5+} from the much shorter and therefore more covalent Tc–O bond. The relevant interatomic distances are presented in Table 2.

Like $Cd_2Re_2O_7$, the new compound $Cd_2Tc_2O_7$ is a colored oxide with metallic luster. The color of $Cd_2Tc_2O_7$ is blue-green, whereas that of the Re analogue is purple.[15] The diffraction results support a stoichiometric oxide with Tc^{5+} cations. Excluding salts of $[TcX_6]^-$ anions, the only other known solid-state compounds containing Tc^{5+} are the yellow pentafluoride

Table 1 Structural parameters for $Cd_2Tc_2O_7$ from Rietveld refinement with high-resolution XRD data at room temperature. Standard uncertainties, which represent $\pm 1\sigma$, are shown in parentheses. The space group $Fd\bar{3}m$ (227) was used with lattice parameter $a = 10.18118(1)$ Å and $Z = 8$ formula units. Atomic displacement parameters U_{iso} are given in Å^2

Atoms	site	x	y	z	U_{iso}
Cd	16*d*	1/2	1/2	1/2	0.0160(2)
Tc	16*c*	0	0	0	0.0096(1)
O	48*f*	0.3175(2)	1/8	1/8	0.017(1)[a]
O′	8*b*	3/8	3/8	3/8	0.009(1)

[a] Anisotropic atomic displacement parameters for O: $U_{11} = 0.021(1)$, $U_{22} = 0.015(1)$, $U_{33} = 0.015(1)$; $U_{12} = 0.0$, $U_{13} = 0.0$, $U_{23} = 0.002(1)$.

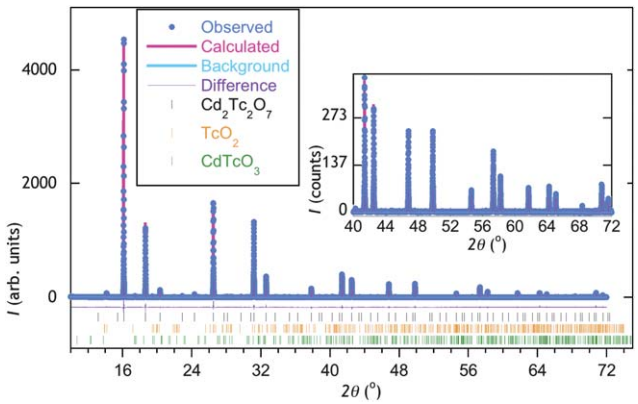

Fig. 1 Observed and calculated XRD powder profiles for $Cd_2Tc_2O_7$ with the difference curve shown below. Reflection marks are shown for $Cd_2Tc_2O_7$ and impurity phases. Inset shows a zoomed-in section of the powder patterns at higher 2θ. The wavelength of the X-rays is $\lambda = 0.82654$ Å.

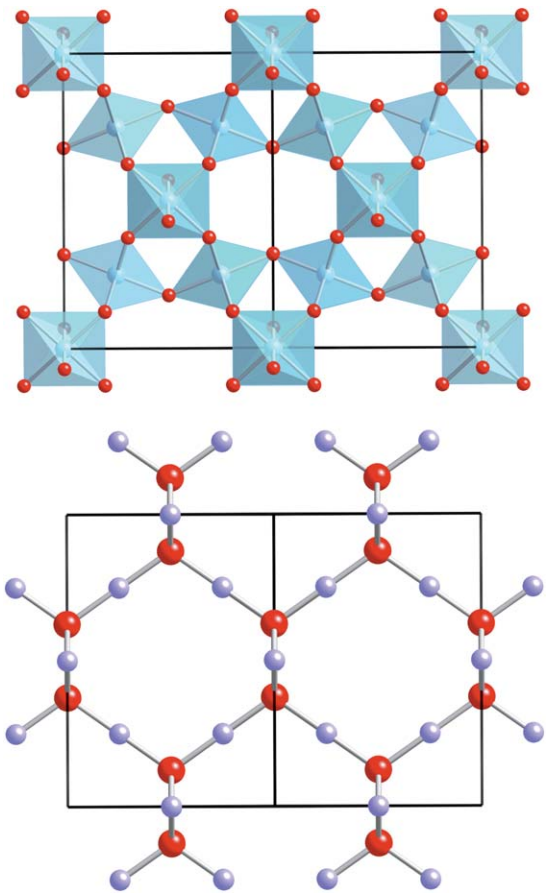

Fig. 2 The crystal structure of $Cd_2Tc_2O_7$ showing the Tc_2O_6 sublattice (top) and the Cd_2O sublattice (bottom).

TcF_5,[20] the oxyhalides $TcOCl_3$ and $TcOBr_3$,[21] and the alkaline oxides Li_3TcO_4 and $NaTcO_3$.[22] However, the crystal structures of these compounds were never determined. Therefore, the Shannon radius for Tc^{5+} was extrapolated from the orthorhombic cell of TcF_5, which is thought to be isostructural to CrF_5.[20,23,24] The radius of 0.546 Å for Tc^{5+} from our studies (1.926 − 1.38 = 0.546) seems especially small when compared to the Shannon radius of 0.60 Å, indicating the increased covalency in $Cd_2Tc_2O_7$ compared to the fluoride. The pentavalent state is unusual for Tc and it is remarkable that it does not undergo disproportionation at 800 °C since the pentafluoride decomposes at 60 °C. Furthermore, the preparation did not require high pressures or oxidizing agents, both necessary for the preparation of $Cd_2Ru_2O_7$.[25]

Table 2 Selected interatomic distances (Å) and angles (°) in $Cd_2Tc_2O_7$ from room temperature powder XRD data. Standard uncertainties are shown in parentheses

Tc–O (×6)	1.926(1)
O–Tc–O	92.0(1)
O–Tc–O	88.0(1)
Tc–O–Tc	138.2(1)
Cd–O′ (×2)	2.2043
Cd–O (×6)	2.587(1)
Cd–O′–Cd	109.471(1)

While not as common as the $A_2^{3+}M_2^{4+}O_7$ pyrochlores, the $A_2^{2+}M_2^{5+}O_7$ pyrochlores can show a diverse array of physical properties, from ferroelectricity to superconductivity. In the case of A = Cd, the pyrochlore oxides exist for M = Nb, Ta, Re, Ru, Ir, Os, and now Tc. For the d^2 and d^3 systems (almost nothing is known for the d^4 Ir-based pyrochlore[26]), the M–O–M angle is relatively open for a pyrochlore oxide, pointing towards increased hybridization of the M d orbitals and the O p orbitals. The x parameter of the O atom (see Table 1) is close to the extremal value of 0.3125, which leads to regular octahedral geometry around the M cations.[7] These values, along with those of the M–O bond distance, are shown for $Cd_2Tc_2O_7$ and related oxides in Table 3. As can be seen from these values, one would expect high covalency in these Cd-based pyrochlores since they have short M–O bond lengths and are close to possessing true octahedral geometry.

When TcO_2 was reacted with CdO, the perovskite phase $CdTcO_3$ was prepared. This is in contrast to the same reaction with PbO which led to the oxygen deficient pyrochlore phase instead. This observation can be understood by considering the differences in the calculated densities between the two Cd–Tc–O phases. For $Cd_2Tc_2O_7$ the calculated density from the XRD data was 6.655 g cc^{-1} and for $CdTcO_3$ 7.556 g cc^{-1}. Therefore, the more ionic, close-packed structure of the perovskite $CdTcO_3$ is found to be more stable than a defect pyrochlore of the type $Cd_2Tc_2O_{6+x}$. This suggests that the high covalency between the Tc^{5+} cations and O anions achieved by the high valency of the Tc cations is necessary to form the pyrochlore phase in the Cd–Tc–O system.

Table 3 The O x parameter and selected bond distances (Å) and angles (°) for $Cd_2Tc_2O_7$ and closely related oxides

Parameter	$Cd_2Tc_2O_7$	$Cd_2Re_2O_7$	$Cd_2Ru_2O_7$	$Cd_2Os_2O_7$
M–O	1.926(1)	1.938(2)	1.924(1)	1.928(1)
M–O–M	138.2(1)	137.7(4)	137.1	137.5(7)
O x parameter	0.3175(2)	0.3184(7)	0.3194(5)	0.319(2)
Ref.	This work	He *et al.*[16]	Wang and Sleight[25]	Mandrus *et al.*[13]

Starting with the structural parameters of $CdTiO_3$, which has the $GdFeO_3$-type structure (see Fig. 3), the Rietveld refinement with the 30 keV XRD data of $CdTcO_3$ converged to the parameters shown in Table 4 with an R_{wp} of 10.8% and χ^2 of 1.993. Again, due to the high-resolution, low-background quality of the data, the R_{wp} is high but both the value of χ^2 and the relatively smooth difference curve between the observed and calculated profiles shown in Fig. 4 support the accuracy of our structural model. Two impurities were readily seen in the high-resolution data with TcO_2 accounting for 2.82 wt.% and CdO 1.28 wt.%. Relevant bond distances and bond angles are shown in Table 5.

The structure of $CdTcO_3$ has orthorhombic symmetry *Pbnm* and the symbol $a^+b^-b^-$ under the Glazer scheme for labeling tilting of the BO_6 octahedra in ABO_3 perovskites.[27,28] The effect of the A cation on the Tc–O bonding in these materials can be understood by comparing some key structural data. For oxides with the perovskite structure the tolerance factor, $t = \langle A\text{–}O\rangle / \sqrt{2}\langle B\text{–}O\rangle$, gives an indication on how distorted the structure is from the ideal perovskite, which has a $t = 1$. Other good measures of these distortions are the M–O–M bond angles and the variation in the oxygen coordination around the A cation. These values and the average M–O distances are listed for $CdTcO_3$ and the closely related oxides of Ti^{+4} and Ru^{+4} with divalent cations in Table 6. One factor influencing the structure is simply one of cation size; in $CdTcO_3$ the octahedral network is more collapsed due the smaller Cd^{2+} (131 pm for 12 CN) when compared to that of $CaRuO_3$ where the bigger Ca^{2+} (134 pm for 12 CN) causes it to be closer to the idealized perovskite structure ($t = 1$). The second factor is related to the electronegativity of Cd.

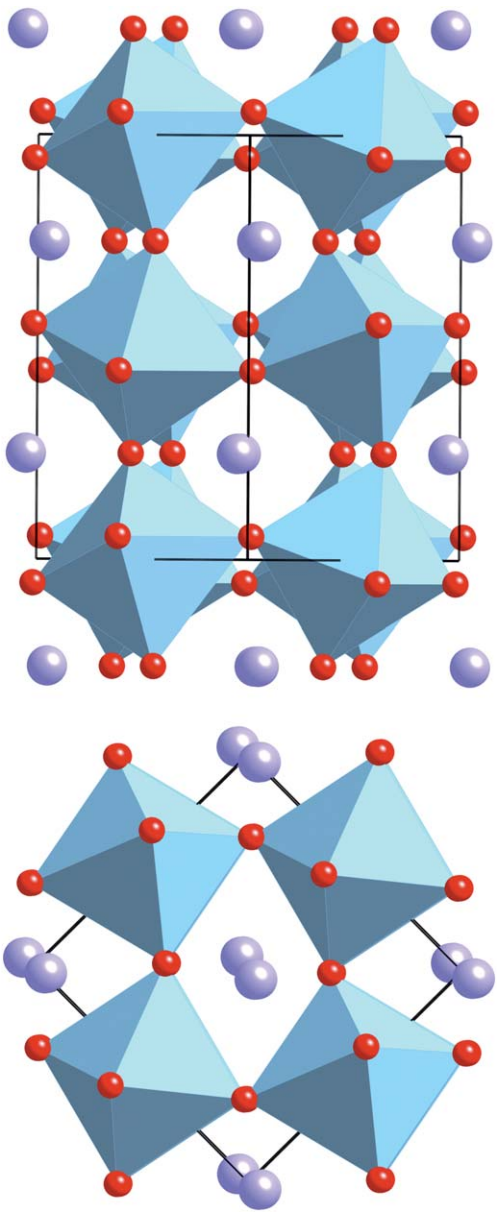

Fig. 3 (Top) The crystal structure of $CdTcO_3$ viewed down one of the body diagonals and (bottom) one of the cell faces. Cadmium cations are shown in purple and TcO_6 octahedra in blue with red O atoms.

Table 4 Structural parameters for $CdTcO_3$ from Rietveld refinement with high-resolution XRD data at room temperature. The lattice is orthorhombic with cell parameters $a = 5.38881(1)$ Å, $b = 5.46504(1)$ Å, and $c = 7.71272$ Å, space group *Pbnm* (62), and $Z = 4$ formula units per cell. Atomic displacement parameters are given in Å^2 and standard uncertainties are shown in parentheses

Atoms	site	x	y	z	U_{iso}
Cd	4*c*	−0.0088(1)	0.04435(4)	1/4	0.0076(1)
Tc	4*b*	1/2	0	0	0.0023(1)
O1	8*d*	0.6844(4)	0.2987(4)	0.0551(3)	0.013(1)
O2	4*c*	0.098(1)	0.458(1)	1/4	0.008(1)

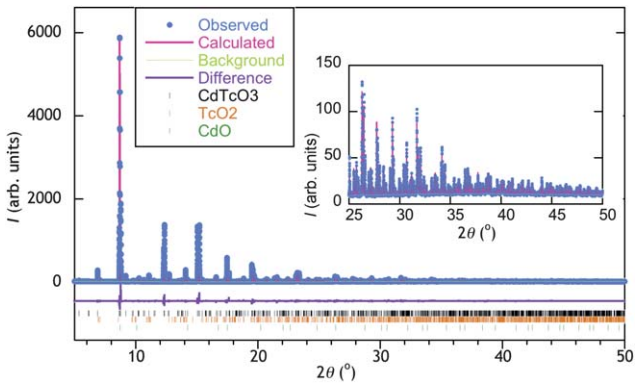

Fig. 4 Observed and calculated XRD powder profiles for $CdTcO_3$ with the difference curve shown below. Reflection marks are shown for $CdTcO_3$ and impurity phases. Inset shows a zoomed-in section of the powder patterns at higher 2θ. The wavelength of the X-rays is $\lambda = 0.41326$ Å.

Table 5 Selected interatomic distances (Å) and angles (°) in $CdTcO_3$ from room temperature powder XRD data. Standard uncertainties are shown in parentheses

Tc–O1 (×2)	1.957(2)	Cd–O2	2.261(3)
Tc–O1 (×2)	2.070(2)	Cd–O2	2.333(3)
Tc–O2 (×2)	2.013(1)	Cd–O2	3.212(3)
⟨Tc–O⟩	2.013(1)	Cd–O2	3.257(3)
Tc–O–Tc	144.7(1)	Cd–O1(×2)	2.226(2)
	146.6(1)	Cd–O1(×2)	2.632(2)
O1–Tc–O2	91.2(1)	Cd–O1(×2)	2.713(2)
O1–Tc–O2	92.4(1)	Cd–O1(×2)	3.480(2)
O1–Tc–O2	91.06(4)	⟨Cd–O⟩	2.764(2)

Table 6 Various structural parameters for $CdTcO_3$ and structurally related perovskites. The parameters include tolerance factor t (see text), the distortion of A cation environment $(A–O)_{var} = (A–O)_{max} - (A–O)_{min}$, and M–O bonding where M is the transition metal. Distances are in Å, angles in °. The values for all the phases are from their room temperature phases, and standard uncertainties are shown in parentheses.

	⟨M–O⟩	M–O–M	$(A–O)_{var}$	t	Ref.
$CdTcO_3$	2.013(1)	144.7(1);146.6(1)	1.254(3)	0.971	This work
$CaRuO_3$	1.991(1)	148.9;150.0	1.144(3)	0.979	Kobayashi *et al.*[29]
$CdTiO_3$	1.9694(4)	150.5(1);149.8(1)	1.084(1)	0.978	Sasaki *et al.*[30]
$CaTiO_3$	1.9503(3)	156.6(1);155.7(1)	0.877(1)	0.986	Sasaki *et al.*[30]

The more electropositive the cation, the more it stabilizes the p orbitals of the O for bonding with the transition metal's d orbitals. In other words, the more ionic the interaction between the A cation and the O anions, the more covalent the interaction between the transition metal and the O atoms. This can be seen from the large Ti–O bond distances in the $CdTiO_3$ than in $CaTiO_3$ (see Table 6). Since Cd has more covalent interactions with the oxygen atoms, as indicated by its more distorted O coordination and shorter Cd–O bond distances, the interaction between Tc and O atoms becomes more ionic.

3.2 Magnetic and electronic properties

The molar magnetic susceptibility χ_{mol} of $Cd_2Tc_2O_7$ with a 5 T applied field is shown in Fig. 5. The susceptibility indicates that $Cd_2Tc_2O_7$ does not display Curie (C/T) or Curie–Weiss ($C/T - \theta$) behavior but instead Pauli paramagnetism above 225 K followed by a drop in χ below 225 K. The SQUID measurement was performed down to 1.8 K; studies below this temperature would determine whether $Cd_2Tc_2O_7$, like $Cd_2Re_2O_7$, also displays superconductivity around 1 K. The sudden drop in susceptibility of $Cd_2Tc_2O_7$ around 4 K may indicate the onset of superconductivity; curiously, this downturn in the magnetic susceptibility is common to several of the oxide samples as seen in Fig. 5.

For comparison with $Cd_2Tc_2O_7$, the magnetic susceptibilities of the isostructural $Pb_2Tc_2O_6$ and $Bi_2Tc_2O_7$ oxides were also measured, as shown in Fig. 5. Contrasting to $Cd_2Tc_2O_7$, $Pb_2Tc_2O_6$ shows a cusp-like transition around 140 K indicative of antiferromagnetic ordering. The low temperature region (below 50 K) for the susceptibility of $Pb_2Tc_2O_6$ shows some Curie behavior, most likely due to impurities. The behavior of $Bi_2Tc_2O_7$ also suggests some type of magnetic ordering below 150 K, albeit one not as sharp as in $Pb_2Tc_2O_6$, possibly due to a second-order type nature of the transition. The possible antiferromagnetic ordering in $Bi_2Tc_2O_7$ and $Pb_2Tc_2O_6$ would be consistent to that observed in other d^3 pyrochlore oxides such as $Cd_2Os_2O_7$[12] and $Hg_2Ru_2O_7$.[4,5] For the Pb and Bi-based ruthenate pyrochlores, no such changes in their magnetic susceptibilities were observed, and those materials were classified as metallic conductors with Pauli paramagnetism.[31]

It is interesting to compare the known properties of chemical and structurally related oxides to the the pyrochlore technetates. The only insulating $Cd_2M_2O_7$ pyrochlores are those for M = Nb and Ta since they contain d^0 cations; the rest are conductors with the Os-based one showing an MI transition around 225 K,[12]

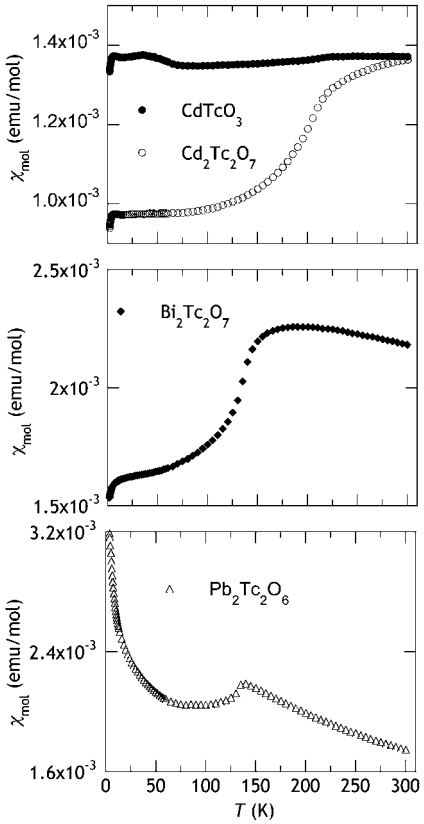

Fig. 5 Molar magnetic susceptibility of $CdTcO_3$ in closed circles, $Cd_2Tc_2O_7$ in open circles, $Bi_2Tc_2O_7$ in closed diamonds, and $Pb_2Tc_2O_6$ in open triangles. The samples were cooled with no field down to 10 K where the field was turned on upon cooling down to 2 K; the susceptibility was then measured upon heating up to 300 K under 5 T field.

which is accompanied by an antiferromagnetic ordering as evidenced by magnetic susceptibility data.[12,13] The magnetic ordering in $Cd_2Os_2O_7$, however, was not detected by temperature dependent NPD measurements, indicating that the ordering occurs locally and never manifests into long-range order.[32] Furthermore, the MI transition in $Cd_2Os_2O_7$ occurs without a crystallographic phase transition and is continuous. Measurements of physical properties such as specific heat further support a second-order transition.[13,33] Singh *et al.* suggest through electronic structure calculations that the magnetic transition in $Cd_2Os_2O_7$ is due to the d^3 state, which lies at a higher density of states at the Fermi level, leading to a magnetic instability.[34] Likewise, the reason why the pyrochlores $Pb_2Tc_2O_6$ and $Bi_2Tc_2O_7$ appear to order magnetically while $Cd_2Tc_2O_7$ does not may have to do with the fact that Tc is in a d^3 configuration in the first two while d^2 in $Cd_2Tc_2O_7$.

In contrast to the MI transition in $Cd_2Os_2O_7$ at 225 K, a second-order transition in $Cd_2Re_2O_7$ occurs at 200 K whereby the electrical resistivity decreases continuously down to low temperatures,[11,35] until a superconducting state is reached around 1.1 K.[9,10] Although believed to be a purely electronic transition at first, careful single crystal studies revealed a cubic-to-tetragonal and centrosymmetric-to-noncentrosymmetric change coinciding with the drop in resistivity and magnetic susceptibility at 200 K.[35,36] Although much less studied, $Cd_2Ru_2O_7$ also displays

similar features in the magnetic susceptibility data with similar transitions occurring at 100 K instead.[25] Furthermore, $Cd_2Ru_2O_7$ is also a metallic conductor, but no one has reported its resistivity below 5 K to check for superconductivity.

For our compound $Cd_2Tc_2O_7$, the magnetic susceptibility data shows similar features to those of $Cd_2Re_2O_7$ as shown in Fig. 5. As observed for $Cd_2Re_2O_7$, the Tc analogue loses its magnetization by about 25–35% at low temperatures. The density of states (DOS) for $Cd_2Tc_2O_7$ from our LMTO calculations support conductivity since the Fermi level is located in the t_{2g} band of Tc, as shown in Fig. 6. Since Tc^{5+} is d^2, the t_{2g} manifold should be about a third filled. Indeed, the calculated DOS shows the Fermi level to be in a valley located between two of the three 'peaks' of the t_{2g} band. Singh *et al.*[34] calculated a similar electronic DOS for $Cd_2Re_2O_7$ where the Fermi level lies in a pseudogap that is a third of the way in the t_{2g} band, suggesting semimetallicity. This could explain the observed blue-green and red colors in $Cd_2Tc_2O_7$ and $Cd_2Re_2O_7$, respectively, where interband transitions between the filled *d*-states and the conduction electrons lead to a plasmon absorption band in the visible range as observed in copper, gold, and ReO_3.[37]

An interesting inelastic scattering study of $Cd_2Re_2O_7$ shows the formation of Raman-active phonon modes known as Goldstone modes that lead to several structural phase transitions below 200 K and therefore a different electronic state at low temperatures.[38] The space groups of those low-temperature phases of $Cd_2Re_2O_7$ were found to be non-centrosymmetric, an interesting property for a material that is electrically conducting and even superconducting in its ground state.[36,39] No doubt, $Cd_2Tc_2O_7$ along with $Cd_2Ru_2O_7$ merit more careful study to answer these outstanding questions and to better understand the subtle structure-property relationships in 4*d* and 5*d* metal-based pyrochlore oxides.

In contrast to $Cd_2Tc_2O_7$, the molar magnetic susceptibility of $CdTcO_3$, shown in Fig. 5, does not show the broad transition of $Cd_2Tc_2O_7$, and is weakly temperature dependent; this behavior does not suggest an ordering transition between 2 K and 300 K since the susceptibility remains mostly constant. However, this does not rule out antiferromagnetic ordering above room temperature. Therefore, LMTO calculations with spin-polarized Tc atoms were undertaken to make predictions. Comparing the calculated relative energies of the non-spin polarized with those

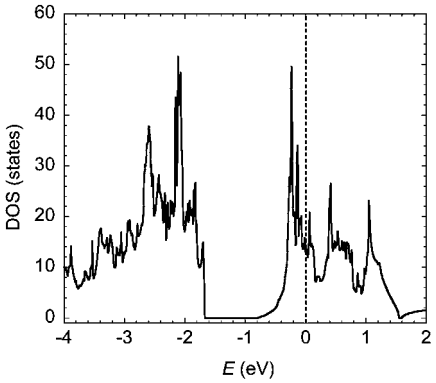

Fig. 6 Calculated densities of states of $Cd_2Tc_2O_7$ with the Fermi energy indicated by the dashed line at 0 eV.

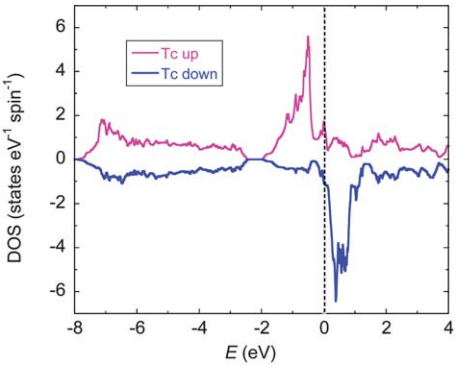

Fig. 7 Calculated densities of states of $Cd_2Tc_2O_7$ with the Fermi energy indicated by the dashed line at 0 eV.

of spin-polarized with ferromagnetic ordering shows the spin-polarized to be more stable by about 0.0357 eV. Another type of magnetic ordering was used in which the moments order antiferromagnetically leading to another lowering of the energy by 0.1818 eV. The resulting DOS of this spin-polarized LMTO calculation with antiferromagnetic ordering is shown in Fig. 7. The DOS plot of $CdTcO_3$ shows the Fermi level above filled *d*-states corresponding to half of the t_{2g} band, so that the other half is left unfilled. These results make sense in light of the fact that in $CdTcO_3$, as in $Pb_2Tc_2O_6$ and $Bi_2Tc_2O_7$, Tc has a d^3 electron configuration. This half-filling of the t_{2g} levels would promote a high-density of states at the Fermi level and therefore a magnetic instability towards ordering.

4 Conclusions and future work

After 40 years of inactivity in the area of ternary technetium oxides, we prepared the bismuth technetates in an earlier study.[6] In the present study we prepare two new technetates with a different post-transition metal–$Cd_2Tc_2O_7$ with the pyrochlore-type structure and $CdTcO_3$ with a distorted perovskite-type structure. For the pyrochlore, no doubt the highly charged Tc^{5+} cations allow the formation of this phase due to the highly covalent nature of the Tc–O bond. This covalency should lead to metallic conductivity in $Cd_2Tc_2O_7$ as is the case in structurally related oxides $Cd_2Re_2O_7$, $Cd_2Ru_2O_7$, and $Cd_2Os_2O_7$. In addition, the calculated DOS of $Cd_2Tc_2O_7$ shows that the Fermi level is in a valley between two high DOS peaks in the t_{2g} band. This leads to the prediction that $Cd_2Tc_2O_7$ should not have a magnetic instability and therefore no magnetic ordering, which accompanies the metal-to-insulator transition in $Cd_2Os_2O_7$. Instead, the behavior of $Cd_2Tc_2O_7$ is much closer to that of $Cd_2Re_2O_7$, a known superconductor where the value of χ_{mol} loses about 30% of its value upon cooling below 200 K.

Future experiments on $Cd_2Tc_2O_7$ and the Ru analogue would establish what role d electron count plays in observing either superconductivity or an MI transitions. Low-temperature (mK range) electrical resistivity measurements or magnetic susceptibility measurements on $Cd_2Tc_2O_7$ would corroborate our prediction of metallicity in these oxides, including a possible superconducting ground-state as implied by our electronic structure calculations and magnetization data. For the perovskite phase $CdTcO_3$, the role of the post-transition metal Cd on

Tc–O bonding and structure become apparent when compared to closely related perovskites such as $SrRuO_3$. In $CdTcO_3$, the more covalent interaction between Cd and O ions and the smaller size of the Cd^{2+} cation lead to a fairly distorted perovskite with Tc–O–Tc bond angles around 145° and an average Tc–O bond length of around 2.07 Å. Nevertheless, our magnetic susceptibility data and electronic structure calculations point towards metallicity in this compound arising from Tc–O bonding.

Acknowledgements

Use of the Advanced Photon Source was supported by the U.S. Department of Energy, Office of Science, Office of Basic Energy Sciences, under Contract No. DE-AC02-06CH11357. Work at Los Alamos was performed under the auspices of the U.S. Department of Energy, Office of Basic Energy Sciences. We would like to thank Brian Toby and Lynn Ribaud from the APS for their help in obtaining the synchrotron XRD data, and Tom O'Dou from the HRC for his valuable help with health physics.

References

1 R. J. Cava, *Dalton Trans.*, 2004, 2979–2987.
2 J. van den Brink, *Nat. Mater.*, 2006, **5**, 427–428.
3 S. Lee, J.-G. Park, D. T. Adroja, D. Khomskii, S. Streltsov, K. A. McEwen, H. Sakai, K. Yoshimura, V. I. Anisimov, D. Mori, R. Kanno and R. Ibberson, *Nat. Mater.*, 2006, **5**, 471–476.
4 W. Klein, R. K. Kremer and M. Jansen, *J. Mater. Chem.*, 2007, **17**, 1356–13600.
5 A. Yamamoto, P. A. Sharma, Y. Okamoto, A. Nakao, H. A. Katori, S. Niitaka, D. Hashizume and H. Takagi, *J. Phys. Soc. Jpn.*, 2007, **76**, 043703.
6 E. E. Rodriguez, F. Poineau, A. Llobet, K. Czerwinski, R. Seshadri and A. K. Cheetham, *Inorg. Chem.*, 2008, **47**, 6281–6288.
7 M. A. Subramanian, G. Aravamudan and G. V. Subba Rao, *Prog. Solid State Chem.*, 1983, **15**, 55–143.
8 K. Lukaszewicz, A. Pietraszko, J. Stepien-Damm and N. N. Kolpakova, *Mater. Res. Bull.*, 1994, **29**, 987–992.
9 R. Jin, J. He, S. McCall, C. S. Alexandar, F. Drymiotis and D. Mandrus, *Phys. Rev. B: Condens. Matter Mater. Phys.*, 2001, **64**, 180503.
10 M. Hanawa, Y. Muraoka, T. Tayama, T. Sakakibara, J. Yamaura and Z. Hiroi, *Phys. Rev. Lett.*, 2001, **87**, 187001.
11 H. Sakai, K. Yoshimura, H. Ohno, H. Kato, S. Kambe, R. E. Walstedt, T. D. Matsuda, Y. Haga and Y. Onuki, *J. Phys.: Condens. Matter*, 2001, **13**, L785–L790.
12 A. W. Sleight, J. L. Gillson, J. F. Wiher and W. Bindloss, *Solid State Commun.*, 1974, **14**, 357–359.
13 D. Mandrus, J. R. Thompson, R. Gaal, L. Forro, J. C. Bryan, B. C. Chakoumakos, L. M. Woods, B. C. Sales, R. S. Fishman and V. Keppens, *Phys. Rev. B: Condens. Matter Mater. Phys.*, 2001, **63**, 195104.
14 E. E. Rodriguez, F. Poineau, A. Llobet, A. P. Sattelberger, J. Bhattacharjee, U. V. Waghmare, T. Hartmann and A. K. Cheetham, *J. Am. Chem. Soc.*, 2007, **129**, 10244–10248.
15 P. C. Donohue, J. M. Longo, R. D. Rosenstein and L. Katz, *Inorg. Chem.*, 1965, **4**, 1152–1153.
16 J. He, R. Jin, B. C. Chakoumakos, J. S. Gardner, D. Mandrus and J. M. Tritt, *J. Electron. Mater.*, 2007, **36**, 740–745.
17 A. C. Larson and R. B. Von Dreele, *General Structure Analysis System (GSAS)*, Los Alamos national laboratory report, laur 86–748 technical report, 2004.
18 A. H. Toby, *Powder Diffr.*, 2006, **21**, 67–70.
19 R. A. Young, *The Rietveld Method*, Oxford University Press, Oxford, 1993, pp. 1–38.
20 A. J. Edwards, D. Hugill and R. D. Peacock, *Nature*, 1963, **200**, 672.
21 R. Colton and I. B. Tomkins, *Aust. J. Chem.*, 1968, **21**, 1981–1985.
22 C. Keller and B. Kanellakopulos, *J. Inorg. Nucl. Chem.*, 1965, **27**, 787–795.
23 D. Babel, *Struct. Bonding*, 1967, **3**, 1–87.
24 R. D. Shannon, *Acta Crystallogr., Sect. A: Cryst. Phys., Diffr., Theor. Gen. Crystallogr.*, 1976, **32**(5), 751–767.
25 R. Wang and A. W. Sleight, *Mater. Res. Bull.*, 1998, **33**, 1005–1007.
26 A. W. Sleight, *Mater. Res. Bull.*, 1974, **9**, 1177–1184.
27 M. Glazer, *Acta Crystallogr., Sect. B: Struct. Crystallogr. Cryst. Chem.*, 1972, **28**, 3384–3392.
28 P. M. Woodward, *Acta Crystallogr., Sect. B: Struct. Sci.*, 1997, **53**, 32–43.
29 H. Kobayashi, M. Nagata, R. Kanno and Y. Kawamoto, *Mater. Res. Bull.*, 1994, **29**, 1271–1280.
30 S. Sasaki, C. T. Prewitt and J. D. Bass, *Acta Crystallogr., Sect. C: Cryst. Struct. Commun.*, 1987, **43**, 1668–1674.
31 M. Tachibana, Y. Kohama, T. Shimoyama, A. Harada, T. Taniyama, M. Itoh, H. Kawaji and T. Atake, *Phys. Rev. B: Condens. Matter Mater. Phys.*, 2006, **73**, 193107.
32 J. Reading and M. T. Weller, *J. Mater. Chem.*, 2001, **11**, 2373–2377.
33 W. J. Padilla, D. Mandrus and D. N. Basov, *Phys. Rev. B: Condens. Matter Mater. Phys.*, 2002, **66**, 035120.
34 D. J. Singh, P. Blaha, K. Schwarz and J. O. Sofo, *Phys. Rev. B*, 2002, **65**, 155109.
35 M. Hanawa, J. Yamaura, Y. Muraoka, F. Sakai and Z. Hiroi, *J. Phys. Chem. Solids*, 2002, **63**, 1027–1030.
36 J. P. Castellan, B. D. Gaulin, J. van Duijn, M. J. Lewis, M. D. Lumsden, R. Jin, J. He, S. E. Nagler and D. Mandrus, *Phys. Rev. B: Condens. Matter Mater. Phys.*, 2002, **66**, 134528.
37 J. Feinleib, W. J. Scouler and A. Ferretti, *Phys. Rev.*, 1968, **165**, 765–774.
38 C. A. Kendziora, I. A. Sergienko, R. Jin, J. He, V. Keppens, B. C. Sales and D. Mandrus, *Phys. Rev. Lett.*, 2005, **95**, 125503.
39 J.-I. Yamaura and Z. Hiroi, *J. Phys. Soc. Jpn.*, 2002, **71**, 2598–2600.

